A technique to model the AC response of diffuse layers at electrode/electrolyte interfaces and to efficiently simulate impedimetric biosensor arrays for many analyte configurations

Federico Pittino, Luca Selmi

DIEGM - Università degli Studi di Udine, Udine, Italy

Phone: +39 0432 558261, Email: federico.pittino@uniud.it

Abstract—We describe a technique to overcome the numerical difficulties in the accurate description of the small signal AC response of the thin electrical double layers at the surface of impedimetric biosensor electrodes. The technique significantly reduces the computational burden of the calculation, thus enabling the fast simulation of many analyte configurations.

I. INTRODUCTION

Numerical simulation of electronic biosensors is an emerging research field (e.g. [1], [2], [3], [4], [5], [6], [7]) to support engineering of integrated devices for personalized medicine [8], [9], [10], [11], [12]. Since at high molarity the electrolyte Debye screening length (λ_D) is much shorter than typical sensor dimensions, challenging multiscale-multiphysics simulation problems arise. Issues are especially severe for impedimetric sensor arrays [11], [12] because every electrode has on top a thin electrical double layer (EDL) with rapidly changing ion concentrations (n_m) and potential (ϕ) [13] which in turn demand either a fine mesh or special purpose boundary conditions [7]. To make things even worse, very accurate calculations are necessary because the useful signal is a small change of the electrode admittance with respect to a reference condition ($\Delta Y = Y - Y_0$) due to changes of the analyte configuration (e.g. introduction of a biomolecule, drift of a biomolecule's position with respect to the electrode, etc.).

In this paper we propose a technique to efficiently account for the EDLs in computing the small signal AC response of impedimetric sensors [11], [12]. The technique significantly reduces the need of fine meshing the EDLs, thus enabling fast simulation of many analyte configurations.

II. METHODOLOGY

We illustrate the method with reference to the nanoelectrode array biosensor presented in [11] (Fig.1), and we use the 3D numerical model of [14] to prove the effectiveness of the proposed approach. The electrode admittance (Y) is computed solving the Poisson-Drift-Diffusion (otherwise denoted Poisson-Nernst-Planck, PNP) equations for small signal sinusoidal excitation [14]. The array behaves as a multiterminal device (Fig.2a), and due to the small λ_D accurate simulations require a very fine mesh next to each electrode, especially at low frequency.

To gain a first insight into the problem, we make use of the analytical 1D model of the electrode response presented in [1] (see Fig.1, left), which states that the admittance per unit area between two electrodes at a distance $L \gg \lambda_D$ with a symmetric 1:1 electrolyte in between, can be written as:

$$y_{tot} = j\omega\varepsilon \frac{\kappa}{2\xi + j\omega\kappa L}(\xi + j\omega) \tag{1}$$

where $\kappa^2 = (\xi + j\omega)/D$ is the squared inverse screening length, $\xi = 2q^2\mu n_0/\varepsilon$ the electrolyte cut-off angular frequency, μ the ion mobility (in m/Ns), $D=\mu kT$ the diffusivity, n_0 the bulk ion concentration. Note that $\lambda_D = \Re(1/\kappa)$. We immediately see that Eq.1 can be rewritten as :

$$\frac{1}{y_{tot}} = \frac{2}{y_{dl}} + \frac{1}{y_{hf}} \quad , \tag{2}$$

where $y_{hf} = (\xi + j\omega)\varepsilon/L$ is the high frequency limit of the electrode admittance, and:

$$y_{dl} = j\omega\varepsilon\kappa \frac{\xi + j\omega}{\xi} \tag{3}$$

is the double layer admittance. Eq.3 shows that y_{dl} is inversely proportional to the scale length $1/\kappa$ which provides an estimate of the thickness of the EDL. The double layer capacitance $c_{dl} = \Im(y_{dl})/\omega$ has a $\omega^{3/2}$ dependence and tends to infinity at high frequency, whereas y_{hf} tends to a constant capacitance per unit area $c_{hf}=\epsilon/L$. These observations suggest to represent the EDL as a lumped admittance in series to an electrode in direct contact to the bulk electrolyte. This representation can be generalized to a multiterminal nanoelectrode array as described in the next paragraphs.

Firstly, we group the array electrodes as follows (Fig.1 right and Fig.2): the grounded ones are connected to terminal C. Among the remaining N electrodes (which we assume all
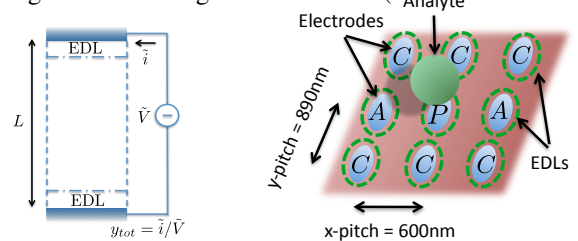
Figure 1: Left: Sketch of the 1D system solved for by the analytical model, Eqs.1,3. Right: Nanoelectrode array sensor. Electrode radius r_{el}=75 nm [11].

biased at the same DC and AC voltage, as in [11]), we group in terminal P those whose EDL is affected by changes in the analyte configuration, while the others are grouped in terminal A. Detailed knowledge of the ion concentrations n_m and potential ϕ in the EDL for all analyte configurations is thus necessary only for electrodes which belong to set P; not for those of set A. In fact, by definition, the EDLs of electrodes in C and A stay the same for all configurations. Note that if the analytes are smaller than the electrode pitch, and with a proper definition of the configuration space, P cointains only one electrode, whereas the A set groups many of them. We now denote M the terminal where the AC current, hence, the admittance is measured, and we start assuming that $M = P$. We will then discuss the case when M is in group A.

The definitions above allow us to model the device as a 2-port with admittance matrix:

$$\mathbf{Y}_2 = \begin{bmatrix} Y_{PP} & Y_{PA} \\ Y_{AP} & Y_{AA} \end{bmatrix} = \begin{bmatrix} \sum_{j\in P}\sum_{l\in P} Y_{jl} & \sum_{j\in P}\sum_{l\in A} Y_{jl} \\ \sum_{j\in A}\sum_{l\in P} Y_{jl} & \sum_{j\in A}\sum_{l\in A} Y_{jl} \end{bmatrix}$$

where the Y_{jl} are the elements of the device N-port $\mathbf{Y}$ matrix.

As suggested by Eq.2, we write the k-th electrode admittance, Y_k ($k \in P$), as the series connection of the EDL admittance, Y_{dlk}, given by the rapidly space-varying field near the electrode, and the bulk admittance, Y_{bk}, given by the field that deeply penetrates into the electrolyte:

$$\frac{1}{Y_k} = \frac{1}{Y_{dlk}} + \frac{1}{Y_{bk}} \quad . \tag{4}$$

The Y_{dlk}s can be computed once for all analyte configurations. We transform the 2-port into a new 2-port with admittance matrix $\mathbf{Y}_{2i}$ connected to the admittances Y_{dlC}, Y_{dlA} (Fig. 2c), respectively representing the EDLs of the electrodes in groups C and A. Clearly, only $\mathbf{Y}_{2i}$ is affected by changes in the analyte configuration, whereas Y_{dlA} and Y_{dlC} are not.

If ports $M=P$ and A are both biased at V_H, the admittance between port M and ground is $Y=Y_{PP}+Y_{PA}$. To identify the unknown admittances Y_{dlC} and Y_{dlA} and then calculate Y for all configurations of interest, we can thus proceed as sketched in Fig.3; namely:
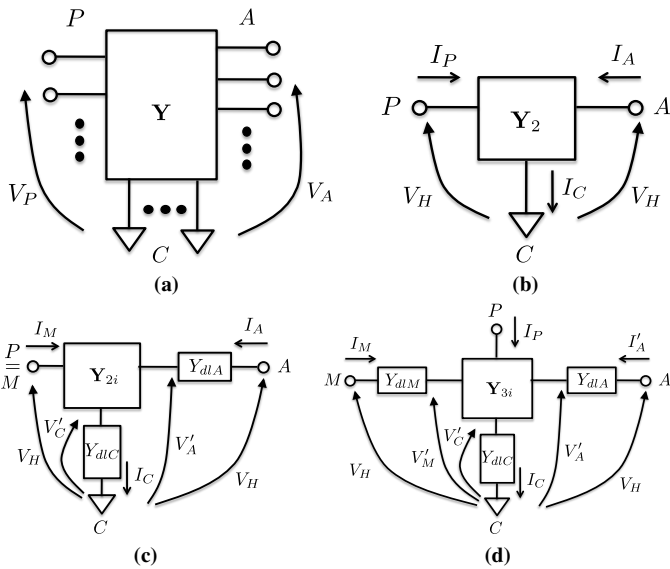
Figure 2: AC small signal representations of the nanoelectrode array: (a) multi-terminal; (b) 2-port; (c) 2-port with external lumped elements ($M = P$); (d) 3-port with external lumped elements ($M \neq P$).

1) we extract the k-th terminal double layer admittance Y_{dlk} in the reference configuration using Eq.4 where $1/Y_{bk}$ the admittance obtained when the EDL is eliminated by setting Dirichlet boundary conditions (DBCs). If the electrodes are all identical (as is typically the case in regular arrays [11], [12]), we can then easily calculate Y_{dlA} and Y_{dlC} as the parallel connection of an appropriate number of Y_{dlk};

2) we set DBCs at all terminals except M (which eliminates the corresponding EDLs and the need for a fine mesh next to the electrodes) and compute the intrinsic $\mathbf{Y}_{2i}$;

3) according to the model of Fig.2c, and denoting Δ the determinant of $\mathbf{Y}_{2i}$, $Y_{iP} = Y_{iPP}+Y_{iPA}$ and $Y_{iA} = Y_{iAP}+Y_{iAA}$, we compute the admittance at M as:

$$Y \approx Y' = Y_{dlC}\frac{\Delta + Y_{iP}\,Y_{dlA}}{\Delta + Y_{iAA}\,Y_{dlC} + Y_{dlA}\,(Y_{iA} + Y_{iP} + Y_{dlC})} \tag{5}$$

4) we change analyte configuration, go back to steps (2)-(3), where meshing of only one EDL is necessary, and efficiently recompute Y' for the new configuration.

Since the EDLs vanish at small distance from the electrodes, simulations at step (1) can be run (with remarkable time saving) on a small subset of the array and imposing DBC on all electrodes other than k. We emphasize that DC bias, Stern layers [13] and self-assembled monolayers (SAMs, assuming that they are much thinner than the separation between the electrodes) should be included in the simulations used to calculate Y_{dlA} and Y_{dlC}.

Let us now consider the case where M is one of the electrodes in A and it is therefore distinct from P. A 3-port model is now mandatory (Fig. 2d). The system matrix is:

$$\mathbf{Y}_3 = \begin{bmatrix} Y_{MM} & Y_{MP} & Y_{MA} \\ Y_{PM} & Y_{PP} & Y_{PA} \\ Y_{AM} & Y_{AP} & Y_{AA} \end{bmatrix}$$

and the expression for the admittance at M is now:

$$Y \simeq Y''' = (Y_{dlC}Y_{dlM}(Y_{dlA}Y_{iM} + \Delta_{21} + \Delta_{22}))$$
$$/\Big(\Delta + Y_{dlC}\Delta_{22} + Y_{dlM}(Y_{iAA}Y_{dlC}$$
$$+ Y_{dlA}(Y_{iA} + Y_{dlC} + Y_{iP} + Y_{iM}) + \Delta_{11} + \Delta_{12} + \Delta_{21} + \Delta_{22})$$
$$+ Y_{dlA}(Y_{dlC}Y_{iMM} + \Delta_{22} + \Delta_{23} + \Delta_{32} + \Delta_{33})\Big) \tag{6}$$

where Δ is the determinant of $\mathbf{Y}_{3i}$, Δ_{ij} is the determinant of the matrix obtained eliminating row i and column j from the matrix $\mathbf{Y}_{3i}$, $Y_{iM} = Y_{iMM}+Y_{iMP}+Y_{iMA}$, $Y_{iP} = Y_{iPM}+Y_{iPP}+Y_{iPA}$ and $Y_{iA} = Y_{iAM}+Y_{iAP}+Y_{iAA}$. The steps to compute the unknowns in Eq.6 and the Y_{dlA}, Y_{dlM} and Y_{dlC} are the same explained for the two-port case (see also Fig.3).
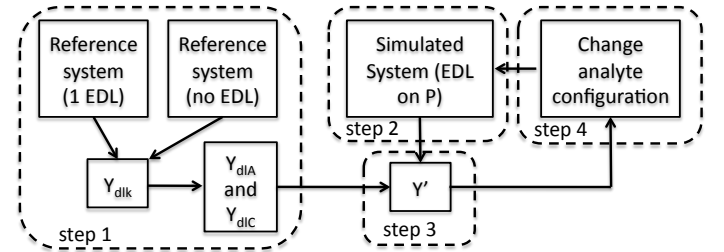
Figure 3: Flowchart of the procedure to calculate Y' when $M=P$. The outer loop on the right (steps 2-4) is repeated for each analyte configuration, while Y_{dlA} and Y_{dlC} are retained. Step 1 is executed only once. Similar procedures are used to calculate Y'' and Y'''.

The method and Eqs.5-6 can be further generalized to cases where the EDLs of more than one active electrode have to be meshed and resolved or when $V_M \neq V_A$. An alternative method, inspired to the mixed mode approach [15], would be to solve the intrinsic system (i.e., with no EDLs on A and C) simultaneously with the equations that give the potential drop on the Y_{dlk}s. The mixed mode approach is fully general and requires to run only one simulation for each analyte configuration (compared to 2 in the 2-port procedure), but it greatly complicates the algorithm implementation and it may introduce numerical issues because the values of the matrix elements in the rows that correspond to the Y_{dlk} are of very different magnitude with respect to those in the rows corresponding to the intrinsic part of the system under study.

III. RESULTS

We tested accuracy and numerical efficiency of the method by investigating the response of the nanoelectrode sensor array in [11], [16] to neutral spherical particles representative of various biomolecules: large proteins ($r_p = 10$nm) [17], viruses ($r_p = 500$ nm) [18], and cylindrical DNA strands ($r_p = 1.25$ nm, h=13.2 nm corresponding to 40 basis) [19].
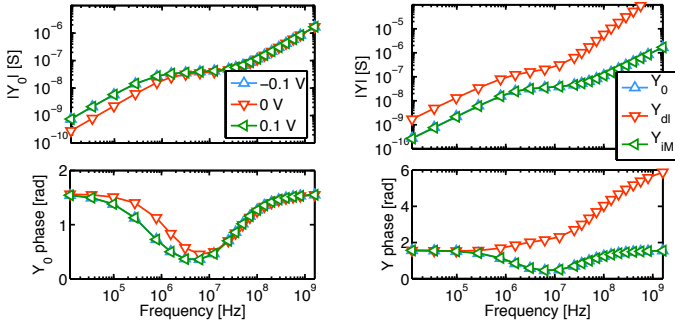
Figure 4: Left: exact total admittance at port $M=P$ in the absence of molecules (Y_0, reference configuration) for a few DC bias voltages. Right: total admittance at port M (Y_0), one-electrode EDL admittance (Y_{dl}), and intrinsic admittance at port M (Y_{iM}). DC bias V_{DC}=0 V; NaCl bulk electrolyte concentration n_0=10 mM.
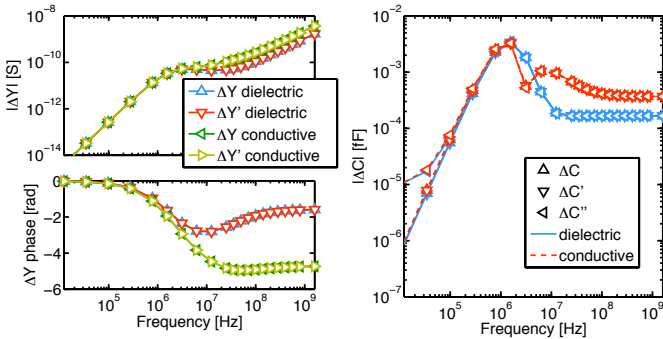
Figure 5: Change in admittance (left) and corresponding change in capacitance (right) due to the introduction of a spherical dielectric or conductive particle (r_p= 10 nm) on the center electrode of the array calculated at $M=P$ with exact 3D simulations (ΔY, ΔC; all EDLs included), with the proposed method ($\Delta Y'$, $\Delta C'$; lumped elements at $k \notin M$) and neglecting EDLs for $k \notin M$ ($\Delta C''$). $\Delta Y'$ and $\Delta C'$ are excellent approximations to ΔY, ΔC at all frequencies. $\Delta Y''$ and $\Delta C''$, instead, deviate at low frequency. Particle height $d_z = 20$ nm; V_{DC}=0 V; n_0=10 mM.

We typically simulate a subset of 5×5 electrodes or less depending on particle size. The molecule is located next to the center electrode (P) and no SAM is present unless otherwise specified.

Fig.4 reports the P-electrode admittance in the absence of molecules (Y_0, reference configuration) calculated with the exact 3D reference model (i.e., with all EDLs included, left, [14]), the intrinsic Y_i (EDL on P only) and the one-electrode EDL admittance Y_{dl} (right). Y_{dl} is comparable to Y at low frequency, whereas $|Y_{dl}| \gg |Y| \simeq |Y_i|$ at high frequency. Fig. 5 shows the change in admittance and in capacitance $\Delta C = \Im(\Delta Y)/\omega$ due to dielectric or metallic particles calculated with the exact 3D model and with the proposed lumped element approximation of the EDLs ($\Delta Y'$). The excellent agreement observed at all frequencies demonstrates the accuracy of the proposed method.

Since at high frequency Y_{dlA} and Y_{dlC} are often much larger than Y, we also computed $Y'' = \lim_{Y_{dlA}, Y_{dlC} \to \infty} Y'$. We see that $Y'' \simeq Y'$ at high frequency, which suggests to further simplify the simulations by neglecting the EDLs on all counterelectrodes except P whenever Y_{dl} is very large, i.e. at large salt concentration and high frequency. The inclusion of Y_{dlA} and Y_{dlC} in the model is instead mandatory for accurate results at low frequency. Similar conclusions were obtained for any particle height, d_z, and radius, r_p, provided the analyte interacts only with electrode P. This is demonstrated in Fig.6, which reports ΔC due to the r_p=500 nm particle in presence
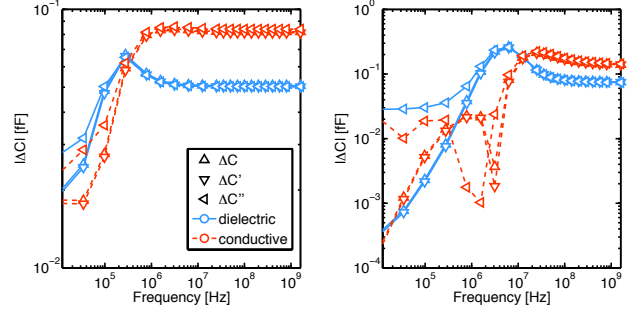
(a) $d_z = 20$ nm, 0.1 mM, DC 0 V **(b)** $d_z = 1$ nm, 10 mM, DC 0.1 V
Figure 6: Change in capacitance due to a spherical dielectric or conductive particle ($r_p = 500$nm) at the center electrode $M=P$ of the array calculated with the reference full 3D simulations (ΔC) and the lumped element model of Fig.2.c ($\Delta C'$ and $\Delta C''$). $\Delta Y'$ and $\Delta C'$ are excellent approximations of ΔY and ΔC at all frequencies; $\Delta Y''$ and $\Delta C''$ only at high frequency. ¿SAM thickness 2.5nm.
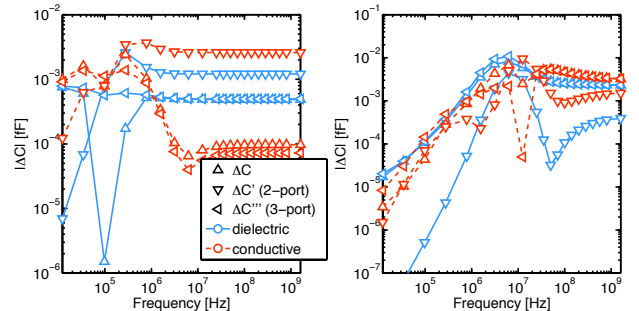
(a) $d_z = 20$ nm, 0.1 mM, DC 0 V **(b)** $d_z = 1$ nm, 10 mM, DC 0.1 V
Figure 7: Same as in Fig. 6, but calculating ΔC at the first neighbour from the central electrode ($M \neq P$). The results given by the 2-port and 3-port models ($\Delta C'$ and $\Delta C'''$) are shown. Note that $\Delta C'''$ is a good approximation of ΔC at all frequencies while $\Delta C'$ is not.

of a 2.5nm thick SAM and for varying position, DC bias and salt concentration.

Fig. 7 shows the results when $M \neq P$ and the 3-port model is used. The comparison with the 2-port approximation (where we included the electrodes P in set A, and calculated Y_{dlA} as the parallel of only those Y_{dl}s that are not in series with P) demonstrates the need of a 3-port representation when $M \neq P$. Fig.8 shows the change in admittance $\Delta Y = Y_{ss} - Y_{ds}$ and capacitance ΔC when a single strand DNA attached to a 2.5 nm SAM on top of the electrode is hybridized with a complementary sequence, thus forming a double strand (ds). The agreement with the reference full 3D simulations is again excellent.

Fig.9 shows the relative speedup between our method and calculations where all EDLs are explicitly meshed for all cases discussed above. A remarkable speedup factor is observed, roughly proportional to the square of the ratio between the number of mesh-points in the systems without and with the lumped elements.

IV. CONCLUSION

A technique is proposed to replace with suitable lumped elements the explicit meshing and simulation of the electrodes' EDLs in array impedimetric sensors. The exact implementation of the method requires careful examination of the physical system, but once the appropriate 2-port or 3-port model has
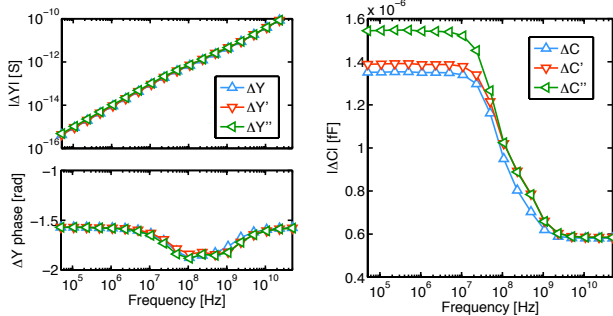
Figure 8: Change in admittance (left) and capacitance (right) due to DNA hybridization. The single (ss) and double (ds) DNA strands are modeled as in [16]. Calculations are done with exact 3D simulations explicitly accounting for all EDLs ($\Delta Y = Y_{ss} - Y_{ds}$, $\Delta C = \Im\left(\Delta Y\right)/\omega$), with the proposed procedure based on lumped elements ($\Delta Y'$, $\Delta C'$) and neglecting all EDLs except the one on $M = P$ ($\Delta Y''$, $\Delta C''$). The DNA is attached to a 2.5 nm SAM and stands upright from the electrode center; n_0=150 mM. $\Delta Y'$ and $\Delta C'$ are excellent approximations to ΔY, ΔC at all frequencies. $\Delta Y''$ and $\Delta C''$ only at high frequency.
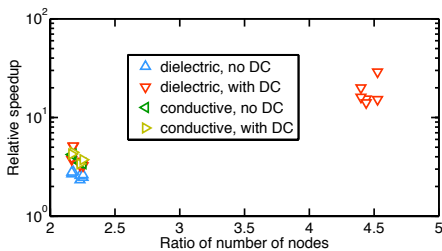
Figure 9: Simulation speedup between the proposed method ($\Delta Y'$, i.e. EDL only on M and lumped elements for $k \notin M$) and the case where all EDLs are explicitly meshed and accounted for (ΔY) versus the ratio of the number of mesh points in the grids. $M = P$. $|V_{DC}|$=0.1 V. The speedup is a factor of 2/3 smaller when $M \neq P$ because one extra simulation is required for each analyte configuration.

been identified, the method offers the possibility to remarkably decrease the mesh size and to accurately examine with largely reduced computational burden many analyte configurations.

V. ACKNOWLEDGMENTS

REFERENCES

[1] F. Pittino, L. Selmi, and F. Widdershoven, "Numerical and analytical models to investigate the AC high-frequency response of nanoelectrode/sam/electrolyte capacitive sensing elements," *Solid-State Electr.*, vol. 88, pp. 82 – 88, 2013.

[2] Y. Wang and G. Li, "Performance investigation for a silicon nanowire fet biosensor using numerical simulation," in *Proc. IEEE Conf. Nano. Mat. Dev.*, 2010, pp. 81–86.

[3] J. L. Gomez and O. Tigli, "Modeling and simulation of zinc oxide nanowire field effect transistor biosensor," in *Proc. IEEE Conf. Nano. Mat. Dev.*, 2011, p. 412.

[4] X. Yang *et al.*, "Simulation of Si nanowire biosensor: Effects of surface and biasing on sensitivity and linearity," in *Proc. IEEE Int. Conf. Nano.*, 2011, pp. 1358–1362.

[5] S. Baumgartner, M. Vasicek, A. Bulyha, and C. Heitzinger, "Optimization of nanowire dna sensor sensitivity using self-consistent simulation," *Nanotechnology*, vol. 22, no. 42, p. 425503, 2011.

[6] A. Hassibi, Y. Liu, and R. Dutton, "Progress in biosensor and bioelectronics simulations: New applications for TCAD," in *Proc. SISPAD*, 2008, pp. 1–4.

[7] S. Baumgartner and C. Heitzinger, "A one-level FETI method for the drift-diffusion-Poisson system with discontinuities at an interface," *J. Comp. Phys.*, vol. 243, pp. 74 – 86, 2013.

[8] J. Bustillo, K. Fife, B. Merriman, and J. Rothberg, "Development of the ion torrent CMOS chip for DNA sequencing," in *Proc. IEDM*, 2013, pp. 196–199.

[9] I. Yanagi *et al.*, "A novel side-gated ultrathin-channel nanopore FET (SGNAFET) sensor for direct DNA sequencing," in *Proc. IEDM*, 2013, pp. 377–380.

[10] C. Toumazou *et al.*, "Simultaneous dna amplification and detection using a ph-sensing semiconductor system," *Nature Methods*, vol. 10, no. 7, pp. 641–646, 2013.

[11] F. Widdershoven *et al.*, "CMOS biosensor platform," *Proc. IEDM*, pp. 816–819, 2010.

[12] C. C. Wong *et al.*, "CMOS based high density micro array platform for electrochemical detection and enumeration of cells," in *Proc. IEDM*, 2013, pp. 373–376.

[13] A. J. Bard and L. R. Faulkner, *Electrochemical Methods: Fundamentals and Applications*, 2nd ed. John Wiley & Sons, 2001.

[14] F. Pittino and L. Selmi, "Use and comparative assessment of the CVFEM method for Poisson-Boltzmann and Poisson-Nernst-Planck three dimensional simulations of impedimetric nano-biosensors operated in the DC and AC small signal regimes," *Computer Methods in Applied Mechanics and Engineering*, 2014. [Online]. Available: doi: 10.1016/j.cma.2014.06.006

[15] J. Rollins and J. Choma, "Mixed-mode PISCES-SPICE coupled circuit and device solver," *Computer-Aided Design of Integrated Circuits and Systems, IEEE Transactions on*, vol. 7, no. 8, pp. 862–867, Aug 1988.

[16] F. Pittino, F. Passerini, P. Palestri, L. Selmi, and F. Widdershoven, "On the response of nanoelectrode capacitive biosensors to DNA and PNA strands," in *Proc. IWASI*, 2013, pp. 40–45.

[17] H. P. Erickson, "Size and shape of protein molecules at the nanometer level determined by sedimentation, gel filtration, and electron microscopy," *Biological Procedures Online*, vol. 11, pp. 32–51, 2009.

[18] R. E. F. Matthews, "A classification of virus groups based on the size of the particle in relation to genome size," *J. Gen. Virol.*, pp. 135–149, 1975.

[19] J. C. G. Montoro and J. L. F. Abascal, "Ionic distribution around simple DNA models. I. Cylindrically averaged properties," *J. Chem. Phys.*, vol. 103, pp. 8273–8284, 1995.